



Universiteit  
Leiden  
The Netherlands

## Development of a near-infrared Raman spectroscopy setup compatible with fluorescence-guided surgery

Abbasi, H.; Lauwerends, L.J.; Schut, T.B.; Santos, I.P.; Caspers, P.J.; Hardillo, J.A.U.; ... ; Puppels, G.J.

### Citation

Abbasi, H., Lauwerends, L. J., Schut, T. B., Santos, I. P., Caspers, P. J., Hardillo, J. A. U., ... Puppels, G. J. (2023). Development of a near-infrared Raman spectroscopy setup compatible with fluorescence-guided surgery. *Analyst*, 148(12), 2676-2682.  
doi:10.1039/d3an00077j

Version: Publisher's Version

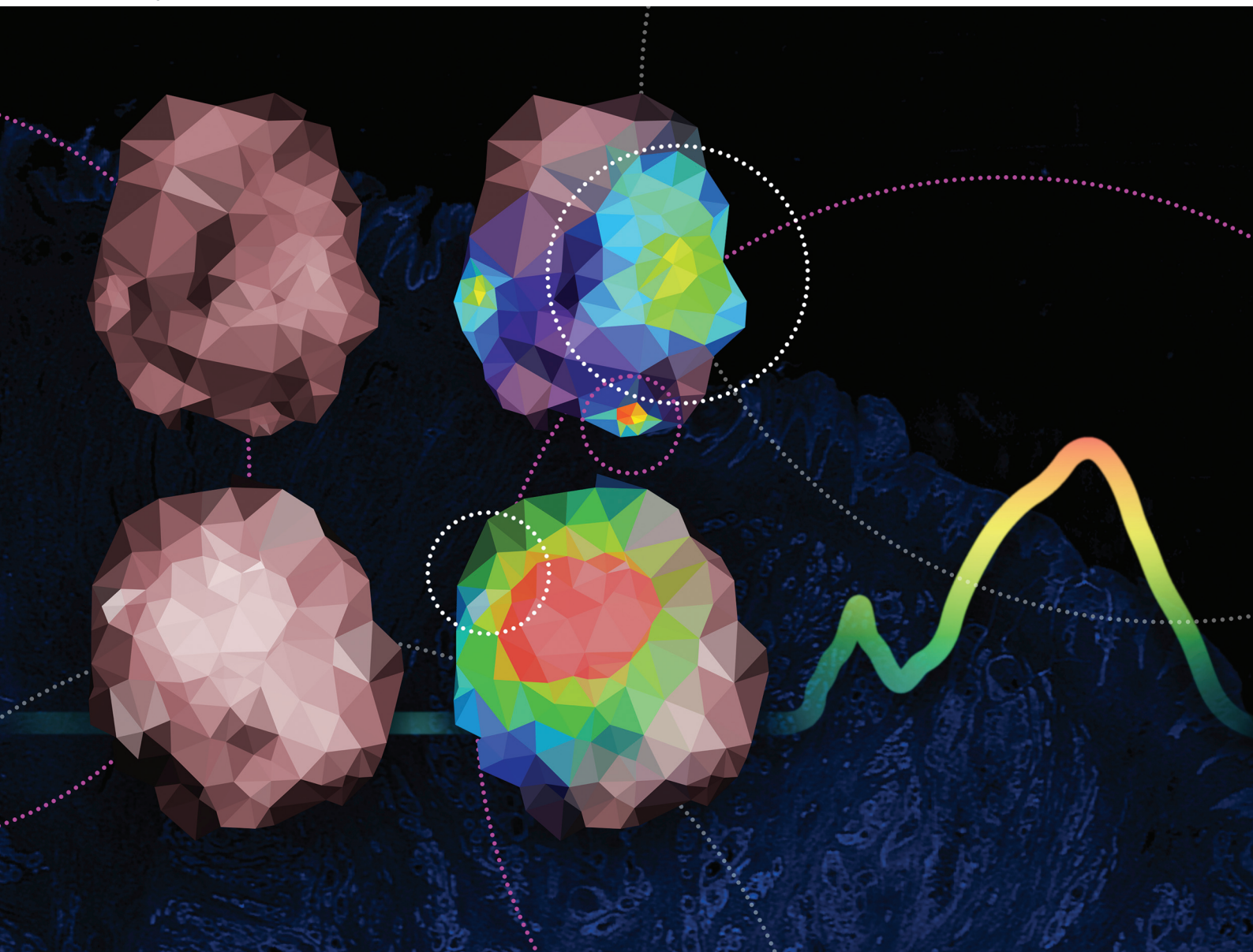
License: [Creative Commons CC BY 4.0 license](https://creativecommons.org/licenses/by/4.0/)

Downloaded from: <https://hdl.handle.net/1887/3762305>

**Note:** To cite this publication please use the final published version (if applicable).

# Analyst

rsc.li/analyst



ISSN 0003-2654

**PAPER**

Hamed Abbasi, Gerwin J. Puppels *et al.*  
Development of a near-infrared Raman spectroscopy setup  
compatible with fluorescence-guided surgery


 Cite this: *Analyst*, 2023, **148**, 2676

## Development of a near-infrared Raman spectroscopy setup compatible with fluorescence-guided surgery

 Hamed Abbasi, <sup>a,b</sup> Lorraine J. Lauwerends, <sup>a</sup> Tom C. Bakker Schut, <sup>b</sup> Inês P. Santos, <sup>c</sup> Peter J. Caspers, <sup>b</sup> Jose A. U. Hardillo, <sup>a</sup> Senada Koljenović, <sup>d</sup> Alexander L. Vahrmeijer, <sup>e</sup> Robert J. Baatenburg de Jong, <sup>a</sup> Stijn Keerweer<sup>a</sup> and Gerwin J. Puppels<sup>\*b</sup>

Near-infrared (NIR) fluorescence imaging using exogenous fluorescent agents provides whole-field images in real-time to assist the surgeon in the excision of a tumor. Although the method has high sensitivity, the specificity can sometimes be lower than expected. Raman spectroscopy can detect tumors with high specificity. Therefore, a combination of both techniques can be advantageous. A complication that must be addressed is that the NIR spectral region is favored by both techniques for (*in vivo*) tissue analysis. When fluorescence and Raman emissions spectrally overlap, it becomes challenging or impossible to detect the Raman signal. In this paper, by avoiding this overlap, we describe a Raman spectroscopy setup capable of recording high-quality Raman spectra from tissue containing NIR exogenous fluorescent agents. We identify an optimal wavelength interval (900–915 nm) for Raman excitation, which avoids both excitation of fluorescent dyes and Raman signal self-absorption by the tissue. In this way, Raman spectroscopy can be combined with the currently most-used NIR fluorescent dyes. This combined novel setup could pave the way for clinical trials benefiting from both fluorescence imaging and Raman spectroscopy to avoid positive margins in cancer surgery.

Received 13th January 2023,

Accepted 8th April 2023

DOI: 10.1039/d3an00077j

[rsc.li/analyst](https://rsc.li/analyst)

### Introduction

Surgery with the aim to remove all tumor tissue is the main treatment modality for most solid cancers. Clear surgical margins are the main prognostic marker for survival in most cases, and inadequate resection generally necessitates adjuvant treatment, associated with increased morbidity, costs, and even mortality. Inadequate resection of the tumor frequently occurs, resulting in positive surgical margins.<sup>1</sup> Although preoperative imaging provides important information on tumor location, surgeons can only rely on visual inspection and palpation to determine the tumor border in the operating room (OR).

Intraoperative optical imaging can provide real-time feedback, aiding in tumor border identification. The combination of whole-field fluorescence-guided surgery (FGS) and Raman Spectroscopy (RS) can be ideal for this purpose.<sup>1–5</sup> FGS using exogenous tumor-specific fluorescent targeting agents has clinically demonstrated benefits for intraoperative margin assessment.<sup>6–12</sup> It facilitates real-time whole-field imaging of the complete surgical field at high sensitivity, but the signal interpretation is complex, and specificity is limited, especially for nonspecific agents. RS, on the other hand, can objectively differentiate between malignant and healthy tissues with high specificity at user-selected locations in the tissue.<sup>13–17</sup> Although these techniques can provide complementary information, they have traditionally been considered mutually exclusive because the low-intensity Raman signal can easily become undetectable in the presence of exogenous fluorophores.

To overcome the interference of intense fluorescence emission, several approaches have been developed, including photo-bleaching,<sup>18</sup> confocal detection,<sup>19</sup> surface-enhanced Raman spectroscopy (SERS),<sup>20</sup> shifted-excitation Raman difference spectroscopy (SERDS),<sup>21–23</sup> polarization-resolved signal detection,<sup>24</sup> and time-resolved signal detection (time gating).<sup>25–27</sup> However, if feasible, the most straightforward way

<sup>a</sup>Fluorescence-Guided Surgery Group, Department of Otorhinolaryngology, Head and Neck Surgery, Erasmus MC Cancer Institute, Rotterdam, Netherlands

<sup>b</sup>Center for Optical Diagnostics and Therapy, Department of Dermatology, Erasmus MC Cancer Institute, Rotterdam, Netherlands.

E-mail: [h.abbasi@erasmusmc.nl](mailto:h.abbasi@erasmusmc.nl), [g.puppels@erasmusmc.nl](mailto:g.puppels@erasmusmc.nl)

<sup>c</sup>Molecular Physical-Chemistry R&D Unit, Department of Chemistry, University of Coimbra, Coimbra, Portugal

<sup>d</sup>Department of Pathology, Antwerp University Hospital/Antwerp University, Antwerp, Belgium

<sup>e</sup>Department of Surgery, Leiden University Medical Center, Leiden, Netherlands

is to avoid the overlap of the RS excitation wavelength and fluorophore absorption wavelengths.<sup>1</sup> This approach was used by Puppels *et al.* in 1993, where lymphocyte subpopulations were selected by means of fluorescence-activated cell sorting (FACS, 488 nm excitation), and Raman spectra were obtained with 660 nm laser excitation, thereby avoiding excitation of the fluorescent labels.<sup>28</sup> More recently, this approach was used to identify breast cancer from the water content in surgical samples containing patent blue dye.<sup>29</sup> While RS using 680 nm laser excitation caused complete obscuration of the Raman signal by the fluorescence of the dye, 785 nm laser excitation allowed differentiation between tumor and healthy tissue in human breast tissue specimens.

Due to the low sensitivity of silicon-based CCD detectors for the wavelength range above 1000 nm, this approach remained mainly limited to the fluorescent materials that emit in the visible range (*e.g.*, photosensitizers: PPIX, Verteporfin, and Temoporfin).<sup>30–33</sup> In 2015, a novel low-noise InGaAs detector enabled the measurement of shot-noise limited Raman spectra in the short-wave infrared (SWIR) region.<sup>34</sup> Excitation with a 976 nm laser allowed RS of otherwise highly fluorescent pigmented skin lesions suspected of melanoma.<sup>35</sup> However, this laser shifts Raman emission in the high wavenumber (HWN) spectral region to around 1.5 micron, where water has a significant absorption band, causing Raman signal absorption.

Tissue water content is an important discriminator between tumor and surrounding healthy tissue and therefore must be measured accurately.<sup>13,36</sup> Therefore, an excitation wavelength long enough to avoid the absorption band of exogenous fluorescent agents whilst being short enough to avoid Raman signal absorption by the tissue is required, including the spectral region of the broad Raman water band between 3150 and 3800  $\text{cm}^{-1}$ . This paper presents the implementation of a 909 nm HWN Raman setup which avoids the absorption band of the most used fluorescent agents and avoids significant tissue self-absorption of Raman signal, thus enabling high-quality Raman spectra measurements of highly fluorescent biological tissues. The performance of the developed setup was tested with phantoms and human tissues containing several exogenous fluorescent agents.

## Methods

### RS systems

Three RS systems were used. The first system (hereafter referred to as 671 nm RS system) was a custom-built multi-channel Raman module (RiverD International B.V., The Netherlands) equipped with a 671 nm laser (Crystalaser, CL671-150-SO). HWN Raman spectra were recorded in the interval from 2500 to 4000  $\text{cm}^{-1}$  using a thermo-electrically cooled ( $-65\text{ }^{\circ}\text{C}$ ) back-illuminated deep depletion CCD (Andor iDus 401, DU401A BR-DD, Andor Technology Ltd, UK). The system was coupled to a fiber-optic needle probe (art photonics GmbH, Germany) described in.<sup>36</sup>

The second system (hereafter referred to as 976 nm RS system) was an SWIR multichannel Raman instrument for measurements in the HWV spectral region, using 976 nm laser excitation.<sup>34</sup>

In the third system (hereafter referred to as 909 nm RS system), the laser of the 976 nm RS system was replaced by a 909 nm laser (Model MDL-III-915L, CNI, China). The angle of the diffraction grating in the spectrometer (BaySpec Inc., San Jose, CA, USA) as well as the position of the detector (Cougar-640, Xenics, Leuven, Belgium) were adjusted to enable measurement of Raman spectra in the HWN spectral region excited by the 909 nm laser. Moreover, as compared to the setup described in,<sup>34</sup> an optical fiber was added to the system. Fig. 1 shows the schematic of the 909 nm RS system.

### Fluorescence imaging systems

Three fluorescence imaging systems have been used in this study. The Quest Spectrum 2.0 (Quest Medical Imaging B.V.), hereafter referred to as the Quest camera, was used for intraoperative *in vivo* imaging in the OR during the resection. The Quest camera was also used for *ex vivo* imaging of resected tissues during residual tissue collection. The Pearl Trilogy (LI-COR Biosciences), hereafter referred to as the Pearl, and the Odyssey CLx Imager (LI-COR Biosciences), hereafter referred to as the Odyssey, were used for *ex vivo* imaging of collected tissues outside the OR.

### Phantoms

An Intralipid 20% emulsion (Fresenius Kabi B.V., Netherlands) was used to compare 909 nm and 976 nm RS systems. Bovine serum albumin (BSA) phantoms with different water mass percentages containing exogenous fluorescent agents were pre-

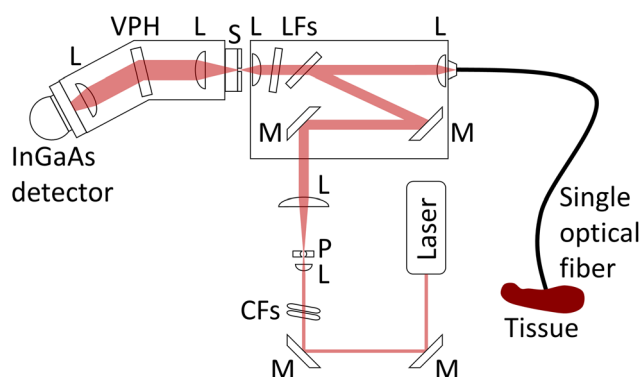


**Fig. 1** Schematic representation of the experimental setup (909 nm RS system). M: mirror, CFs: cleaning filters, L: lens, P: pinhole, LFs: longpass filters, S: slit, VPH: volume phase holographic grating. Single optical fiber (multimode, fused silica, core: 100  $\mu\text{m}$ ) is used for guiding laser light to the tissue and scattered light back from the tissue. As compared to the 976 nm RS system, the spectral laser-cleaning filters and beam expander were changed to match the central wavelength and beam size of the new laser, respectively. A pinhole (diameter: 25  $\mu\text{m}$ ) was also added to the beam expander (Keplerian telescope) to spatially clean the laser beam. The slit was replaced with a wider slit (width: 100  $\mu\text{m}$ ) to avoid aliasing and also to increase the optical throughput of the system.

pared to examine the ability of the 909 nm RS system to determine the water mass percentages. These phantoms comprised of water, BSA (Sigma Chemical Co, USA), and one of three exogenous fluorescent agents, SGM-101, Methylene blue (MB), or Indocyanine green (ICG). MB and ICG are nonspecific fluorescent agent used in intraoperative fluorescence imaging. SGM-101 is a tumor-specific molecule that consists in a CEA-specific, chimeric monoclonal antibody conjugated to a NIR-emitting fluorochrome (BM104).<sup>37,38</sup> BSA mass percentages in the phantoms ranged between 2.5% and 25%, with 2.5% intervals. SGM-101, MB, and ICG were added to final concentrations of 1, 10, and 100  $\mu\text{g ml}^{-1}$  to mimic the reported tissue concentrations of these agents in the tumor during trials of FGS [38–41]. Fig. 2 shows the prepared phantoms.

### Specimen

Residual tissue (superfluous tissue after standard pathology procedures) was collected (without interfering with standard clinical procedures) from six patients with colorectal cancer who had undergone FGS. The study was approved by the local Ethics Review Committee (METC Erasmus MC: MEC-2019-0794), and conducted in full compliance with the laws and regulations of the Netherlands. All pieces of collected residual tissue were checked with the Quest camera for fluorescence signal. Raman measurements on fresh tissues were performed directly after the resection. Raman measurements on frozen tissues were performed after thawing.

## Results and discussion

Amongst all currently clinically approved fluorescent agents and those under clinical development, ICG has the longest absorption wavelength.<sup>1</sup> The 976 nm RS system has an excitation wavelength that is more than 150 nm longer than the absorption peak of ICG. However, the 3150–3800  $\text{cm}^{-1}$  spectral region of the Raman water band overlaps with the NIR water absorption peak between 1400 nm and 1500 nm. This leads to absorption of Raman signal in the tissue, which significantly affects the Raman spectrum. This is illustrated in Fig. 3, which

shows HWN Raman spectra of a phantom (intralipid 20%) collected with the 909 nm and 976 nm RS systems with comparable optical pathways through the sample. Both spectra were recorded using a single optical fiber with a sampling depth of about 250  $\mu\text{m}$ .<sup>39</sup> It makes clear that in applications that aim to determine the water content of tissue, self-absorption of Raman signal must be taken into account and avoided to the extent possible by proper choice of laser excitation wavelength.

For the 909 nm RS system, the HWN Raman spectrum is below 1400 nm where water absorption is negligible. The ICG absorption peak is *ca.* 100 nm shorter than the laser wavelength of the 909 nm RS system; however, the tail of its absorption spectrum reaches the laser wavelength. Therefore, the amount of induced fluorescence in the 909 nm RS system is a function of agent concentration in the tissue. To assess if the

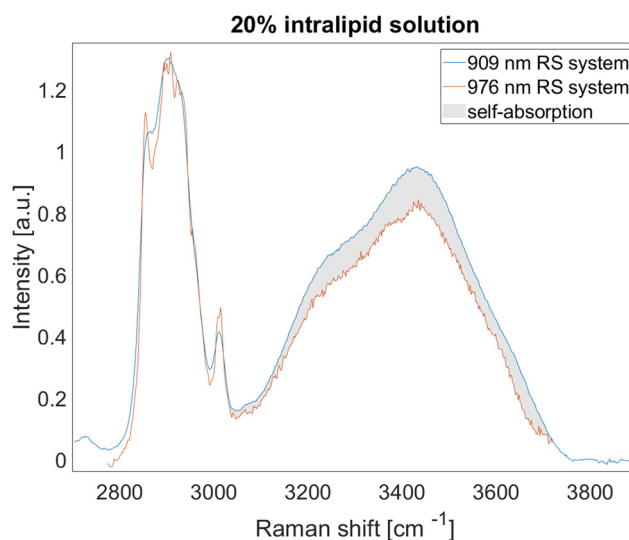


**Fig. 3** Intralipid 20% emulsion measured with 976 nm and 909 nm RS systems (normalized to the CH band). The difference between the observed intensities is mainly due to higher self-absorption of Raman photons excited by the 976 nm laser as compared to the 909 nm laser. The difference in the shape of the peak at the CH-stretching band is due to the wider slit used in the 909 nm RS system.

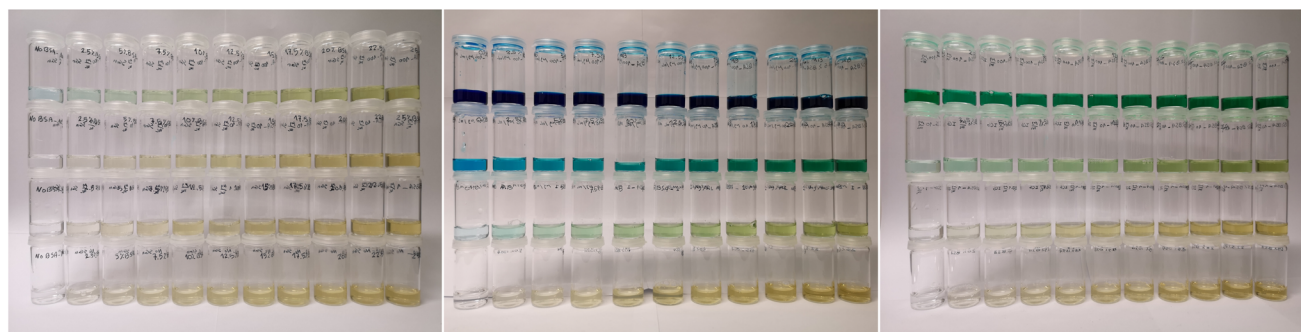


**Fig. 2** Prepared phantoms: SGM-101 (left), MB (middle), and ICG (right). In each row of vials, from left to right, the water percentage is reduced from 100% to 75%, and the BSA percentage is increased from 0% to 25%. The bottom rows are blank solutions (no fluorescent agent). The bottom's second, third, and fourth rows have fluorescent agents' concentrations of 1  $\mu\text{g mL}^{-1}$ , 10  $\mu\text{g mL}^{-1}$ , and 100  $\mu\text{g mL}^{-1}$ , respectively.

induced fluorescence in the 909 nm RS system is negligible, the BSA phantom study was performed with various concentrations of SGM-101, MB, and ICG. Typically, a few milligrams of an agent are pre-operatively administered to the patient; however, a considerable amount of the administered dosage is cleared through the liver (excretion into bile and feces) and/or through the kidney (excretion into urine).<sup>40</sup> Therefore, the absolute concentration of the agent in the target tissue is much lower than the administered dosage. For ICG and other agents (e.g., 5-ALA, and Cetuximab-800CW), absolute concentrations between 1 to 10  $\mu\text{g mL}^{-1}$  are reported.<sup>41–44</sup>

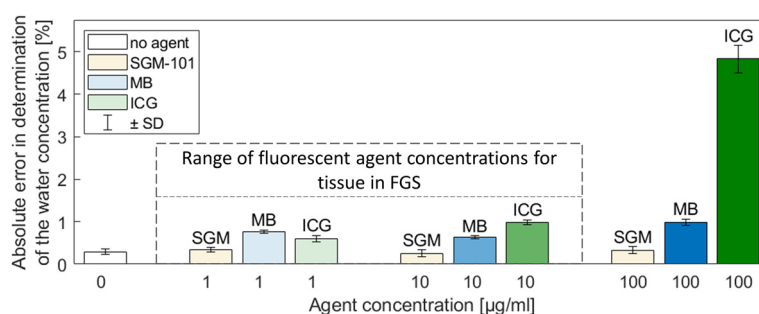
Fig. 4 shows the result of the phantom study where the water concentration in mass percentage of the BSA phantoms was measured in the presence of SGM-101, MB, and ICG at different concentrations. The water concentration of the phantoms was calculated from the ratio of the OH and CH bands, as described by Caspers *et al.*<sup>45</sup> The results of the phantom study showed that in the expected range for absolute concentration in the tissue, the 909 nm RS system can determine the water percentage with an absolute error below 1%. The absolute error was calculated as the difference between the calculated and actual percentages. Therefore, it can be concluded that the fluorescence interference in the 909 nm RS system is negligible.

Table 1 presents the specification of the collected tissues from patients and the utilized experimental systems.

Fig. 5 shows typical HWN Raman spectra measured with 909 nm RS system (top two rows) and 671 nm RS system (bottom row) of tissues resected from FGS containing different fluorescent agents. For each specimen, the measured spectrum including both Raman and fluorescence is shown in the left

box, and the Raman spectrum after subtraction of the fluorescence background is shown in the right box. For tissues measured with the 671 nm RS system (Fig. 5g–i), the Raman signal to fluorescence ratio is very small. This makes proper fluorescence signal subtraction needed for interpretation of the Raman signal unreliable. The 671 nm RS system completely failed to present HWN Raman spectra from tissue containing ICG (g2). In h2 and i2 (cRGD-ZW800-1), the lipid/protein band is not well separated from the water band due to the intense fluorescence seen by the detector in the 671 nm RS system. For tissues measured with the 909 nm RS system (Fig. 5a–f) on the other hand, fluorescence signal background is virtually absent. For each spectrum, the ratio of Raman to fluorescence (R/F) in the CH-stretching band (2910–2966  $\text{cm}^{-1}$ ) is shown. In the spectra measured with the 909 nm RS system, R/F is a few thousand times greater than those measured with the 671 nm RS system.

Typical laser wavelengths used in clinical Raman spectroscopy are 514 nm, 532 nm, 671 nm, 785 nm, 830 nm, 976 nm, and 1064 nm.<sup>46,47</sup> Fig. 6 illustrates the overlap of the fingerprint and HWN Raman spectra of the above-mentioned laser wavelengths as well as the laser wavelength used in the current study (909 nm) with the absorption band of ICG, SGM-101, and water. Raman spectra recorded by lasers with wavelengths below 900 nm would increasingly suffer from intense signal background of fluorescent agents. Although laser excitation wavelengths of 976 nm and higher have been shown to solve the problem of strong fluorescence signal background, its HWN Raman region overlaps with the water absorption peak between 1400 nm and 1500 nm leading to significant tissue self-absorption, which is difficult to correct for.



**Fig. 4** Absolute error in determining the water mass percentage in BSA-water phantoms containing different concentrations of SGM-101, MB, and ICG measured using 909 nm RS system. In the expected concentration of the fluorescent agent in the tissue during FGS, *i.e.*, between 1 to 10  $\mu\text{g mL}^{-1}$ , the 909 nm RS system can determine water mass percentage with an absolute error of less than 1% in all three examined fluorescent agents.

**Table 1** Specification of the collected tissues from patients and the utilized experimental systems

Patient	Tissue type	Agent used in FGS	Fluorescence imaging channel	RS system (tissue condition)
1	Colorectal	SGM-101	700 nm	909 nm (thawed)
2	Colorectal	SGM-101	700 nm	909 nm (thawed)
3	Omental flap (adipose)	ICG	800 nm	909 nm (fresh)
4	Colorectal	cRGD-ZW800-1	800 nm	909 nm (thawed)
5	Colorectal	ICG	800 nm	671 nm (fresh)
6	Colorectal	cRGD-ZW800-1	800 nm	671 nm (fresh)

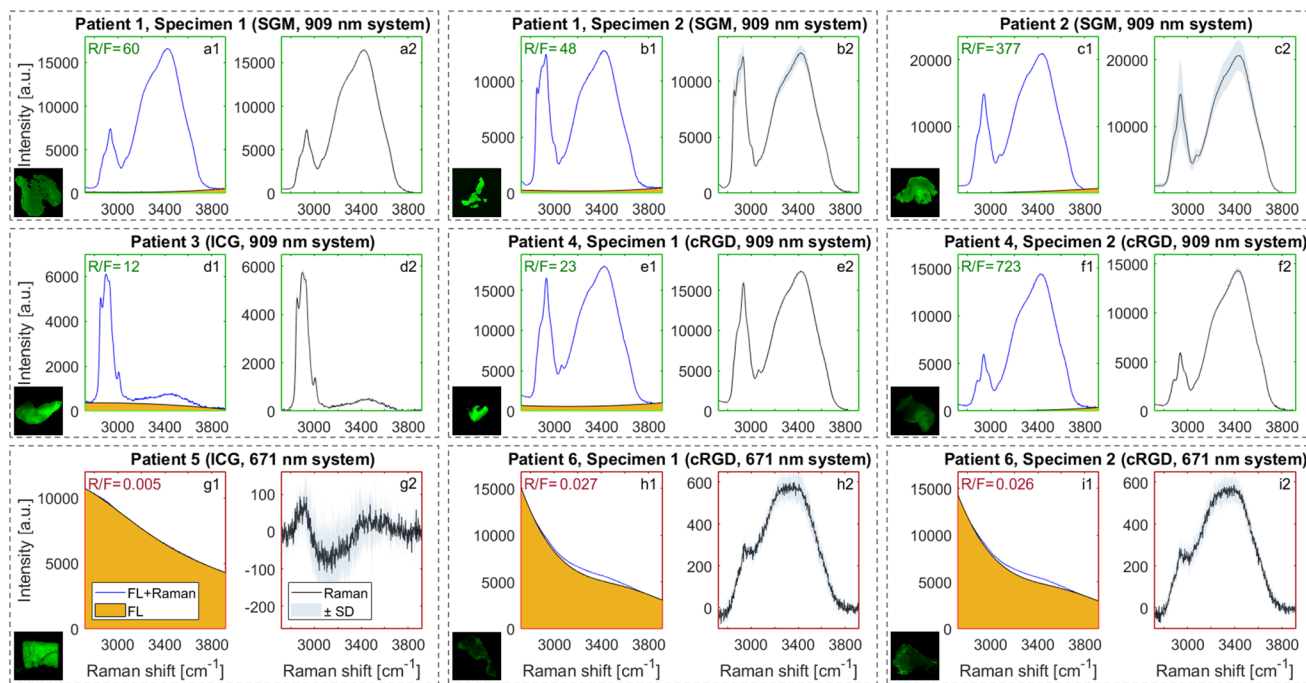


**Fig. 5** Raman spectra of resected tissues from patients treated with FGS using ICG, cRGD-ZW800-1, and SGM-101 measured with 909 nm RS system (a–f) and 671 nm RS system (g–i). For each specimen, a fluorescence image captured by Odyssey/Pearl is shown. Each shown spectrum (for both systems) is an average of 3 recorded spectra. The upper two rows (measured with 909 nm RS system) present very high signal quality.

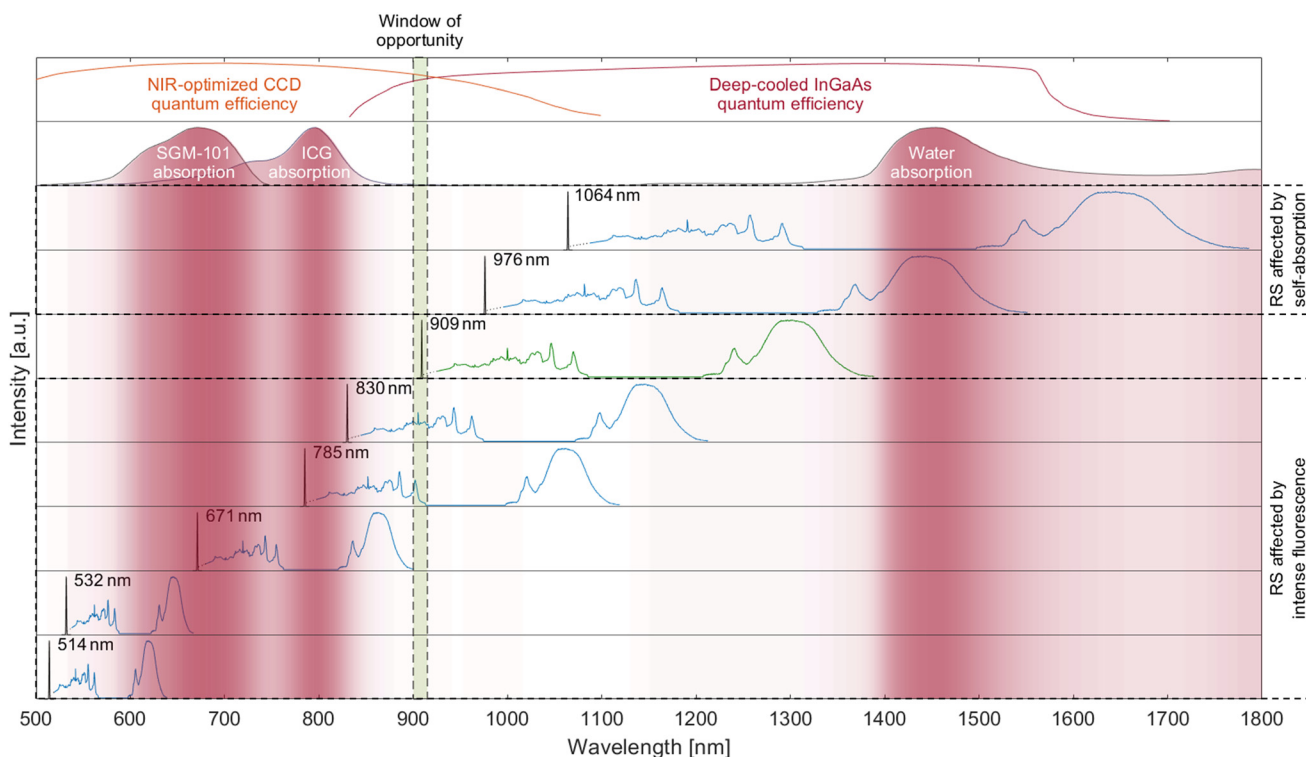


**Fig. 6** Overlap of Raman spectra excited with typical laser wavelengths used in clinical trials, *i.e.*, 514 nm, 532 nm, 671 nm, 785 nm, 830 nm, 909 nm, 976 nm, and 1064 nm with absorption spectra of SGM-101, ICG, and water. A laser wavelength below  $\sim 900$  nm overlaps with the absorption band of exogenous fluorescent agents (left red shaded zones) and consequently hinders Raman signal by photon shot noise originating from exogenous fluorescent agents. Excitation above  $\sim 915$  nm shifts the HWN part of the Raman spectra toward higher water absorption (right red shaded zone), resulting in intense tissue self-absorption.

Therefore, 909 nm is the optimal wavelength which avoids the absorption band of the most used fluorescent agents, including ICG, and avoids significant tissue self-absorption of Raman signal in both fingerprint and HWN regions.

## Conclusions

We demonstrated the first fiber-optic RS setup capable of acquiring high-quality Raman spectra from the resected tumor tissue containing exogenous NIR fluorescent agents (including ICG). High-quality Raman spectra are obtained due to high Raman signal to fluorescence signal ratio. In this setup, the Raman excitation wavelength does not overlap with the absorption band of most used exogenous fluorescent agents, nor does the Raman emission wavelength overlap with the water absorption band, therefore avoiding intense exogenous fluorescence and Raman signal absorption, respectively. In the rapidly growing field of FGS, the complementary information provided by RS can be the long-sought answer to dealing with many of the limitations as described by Keereweer *et al.*<sup>40</sup> This novel setup opens the door to clinical trials benefiting from the complementary use of FGS and RS with the goal of avoiding positive margins in cancer surgery.

## Ethics committee approval

This study was exempted by the Medical Research Ethics Committee (MREC), having concluded that this study is not subject to the Medical Research Involving Human Subjects Act (WMO).

## Conflicts of interest

The authors declare no competing financial interest.

## Acknowledgements

The authors acknowledge the funding of Erasmus MC Foundation through Daniel den Hoed Award for young scientific talent. The authors also acknowledge SurgiMab S.A.S. for providing SGM-101 tracers. They would further like to thank Elisa M. Barroso, Yassine Aaboubout, Hidde A. Galema, Denise E. Hilling, Mahesh Algae, Thierry van den Bosch, and Michail Doukas.

## References

- L. J. Lauwerends, H. Abbasi, T. C. Bakker Schut, P. B. A. A. Van Driel, J. A. U. Hardillo, I. P. Santos, E. M. Barroso, S. Koljenović, A. L. Vahrmeijer, R. J. Baatenburg de Jong, G. J. Puppels and S. Keereweer, *Eur. J. Nucl. Med. Mol. Imaging*, 2022, **49**, 2364–2376.
- S. G. Brouwer de Koning, A. W. M. A. Schaeffers, W. Schats, M. W. M. van den Brekel, T. J. M. Ruers and M. B. Karakullukcu, *Eur. J. Surg. Oncol.*, 2021, **47**, 2220–2232.
- G. Balasundaram, C. Krafft, R. Zhang, K. Dev, R. Bi, M. Moothanchery, J. Popp and M. Olivo, *J. Biophotonics*, 2021, **14**, e202000280.
- L. J. Lauwerends, H. A. Galema, J. A. U. Hardillo, A. Sewnaik, D. Monserez, P. B. A. A. van Driel, C. Verhoef, R. J. Baatenburg de Jong, D. E. Hilling and S. Keereweer, *Cancers*, 2021, **13**, 1895.
- J. Heidkamp, M. Scholte, C. Rosman, S. Manohar, J. J. Fütterer and M. M. Rovers, *Int. J. Cancer*, 2021, **149**, 635–645.
- B. E. Schaafsma, J. S. Mieog, M. Hutteman, J. R. van der Vorst, P. J. Kuppen, C. W. Lowik, J. V. Frangioni, C. J. van de Velde and A. L. Vahrmeijer, *J. Surg. Oncol.*, 2011, **104**, 323–332.
- G. M. van Dam, G. Themelis, L. M. Crane, N. J. Harlaar, R. G. Pleijhuis, W. Kelder, A. Sarantopoulos, J. S. de Jong, H. J. Arts, A. G. van der Zee, J. Bart, P. S. Low and V. Ntziachristos, *Nat. Med.*, 2011, **17**, 1315–1319.
- A. L. Vahrmeijer, M. Hutteman, J. R. van der Vorst, C. J. van de Velde and J. V. Frangioni, *Nat. Rev. Clin. Oncol.*, 2013, **10**, 507–518.
- H. J. M. Handgraaf, M. C. Boonstra, H. Prevoo, J. Kuil, M. W. Bordo, L. S. F. Boogerd, B. G. Sibinga Mulder, C. F. M. Sier, M. L. Vinkenburg-van Slooten, A. Valentijn, J. Burggraaf, C. J. H. van de Velde, J. V. Frangioni and A. L. Vahrmeijer, *Oncotarget*, 2017, **8**, 21054–21066.
- L. S. F. Boogerd, C. E. S. Hoogstins, D. P. Schaap, M. Kusters, H. J. M. Handgraaf, M. J. M. van der Valk, D. E. Hilling, F. A. Holman, K. Peeters, J. S. D. Mieog, C. J. H. van de Velde, A. Farina-Sarasqueta, I. van Lijnschoten, B. Framery, A. Pelegrin, M. Gutowski, S. W. Nienhuijs, I. de Hingh, G. A. P. Nieuwenhuijzen, H. J. T. Rutten, F. Cailler, J. Burggraaf and A. L. Vahrmeijer, *Lancet Gastroenterol. Hepatol.*, 2018, **3**, 181–191.
- L. J. Lauwerends, P. B. A. A. van Driel, R. J. Baatenburg de Jong, J. A. U. Hardillo, S. Koljenovic, G. Puppels, L. Mezzanotte, C. W. G. M. Löwik, E. L. Rosenthal, A. L. Vahrmeijer and S. Keereweer, *Lancet Oncol.*, 2021, **22**, e186–e195.
- J. S. D. Mieog, F. B. Achterberg, A. Zlitni, M. Hutteman, J. Burggraaf, R.-J. Swijnenburg, S. Gioux and A. L. Vahrmeijer, *Nat. Rev. Clin. Oncol.*, 2022, **19**, 9–22.
- E. M. Barroso, R. W. Smits, T. C. Bakker Schut, I. ten Hove, J. A. Hardillo, E. B. Wolvius, R. J. Baatenburg de Jong, S. Koljenovic and G. J. Puppels, *Anal. Chem.*, 2015, **87**, 2419–2426.
- Z. Liao, M. G. Lizio, C. Corden, H. Khout, E. Rakha and I. Notingher, *J. Raman Spectrosc.*, 2020, **51**, 1986–1995.
- I. J. Pence, C. A. Patil, C. A. Lieber and A. Mahadevan-Jansen, *Biomed. Opt. Express*, 2015, **6**, 2724–2737.
- G. Thomas, T. Q. Nguyen, I. J. Pence, B. Caldwell, M. E. O'Connor, J. Giltneane, M. E. Sanders, A. Grau,

- I. Meszoely, M. Hooks, M. C. Kelley and A. Mahadevan-Jansen, *Sci. Rep.*, 2017, **7**, 13548.
- 17 M. Haifler, I. Pence, Y. Sun, A. Kutikov, R. G. Uzzo, A. Mahadevan-Jansen and C. A. Patil, *J. Biophotonics*, 2018, **11**, e201700188.
- 18 H. Wang, J. Zhao, A. M. D. Lee, H. Lui and H. Zeng, *Photodiagn. Photodyn. Ther.*, 2012, **9**, 299–302.
- 19 G. J. Puppels, W. Colier, J. H. F. Olminkhof, C. Otto, F. F. M. de Mul and J. Greve, *J. Raman Spectrosc.*, 1991, **22**, 217–225.
- 20 M. R. Kagan and R. L. McCreery, *Anal. Chem.*, 1994, **66**, 4159–4165.
- 21 M. A. d. S. Martins, D. G. Ribeiro, E. A. Pereira dos Santos, A. A. Martin, A. Fontes and H. d. S. Martinho, *Biomed. Opt. Express*, 2010, **1**, 617–626.
- 22 E. Cordero, F. Korinith, C. Stiebing, C. Krafft, I. W. Schie and J. Popp, *Sensors*, 2017, **17**, 1724.
- 23 F. Korinith, T. A. Shaik, J. Popp and C. Krafft, *Analyst*, 2021, **146**, 6760–6767.
- 24 S. M. Angel, M. K. DeArmond, K. W. Hanck and D. W. Wertz, *Anal. Chem.*, 1984, **56**, 3000–3001.
- 25 P. Matousek, M. Towrie, C. Ma, W. M. Kwok, D. Phillips, W. T. Toner and A. W. Parker, *J. Raman Spectrosc.*, 2001, **32**, 983–988.
- 26 D. V. Martyshkin, R. C. Ahuja, A. Kudriavtsev and S. B. Mirov, *Rev. Sci. Instrum.*, 2004, **75**, 630–635.
- 27 N. Ksantini, I. Veilleux, M.-M. de Denus-Baillargeon, P. Orsini, I. Dicaire, J.-B. Lecourt, A. Gognau, Y. Hernandez, A. Baylon, M. Massabki, F. Lesage and F. Leblond, *J. Biophotonics*, 2022, **15**, e202100188.
- 28 G. J. Puppels, H. S. P. Garritsen, J. A. Kummer and J. Greve, *Cytometry*, 1993, **14**, 251–256.
- 29 T. J. E. Hubbard, A. P. Dudgeon, D. J. Ferguson, A. C. Shore and N. Stone, *Transl. Biophotonics*, 2021, **3**, e202000023.
- 30 C. C. Horgan, M. S. Bergholt, A. Nagelkerke, M. Z. Thin, I. J. Pence, U. Kauscher, T. L. Kalber, D. J. Stuckey and M. M. Stevens, *Theranostics*, 2021, **11**, 2006–2019.
- 31 C. Horgan, M. Bergholt, M. Z. Thin, A. Nagelkerke, R. Kennedy, T. Kalber, D. Stuckey and M. Stevens, *J. Biomed. Opt.*, 2021, **26**, 036002.
- 32 M. C. M. Grimbergen, C. F. P. van Swol, R. J. A. van Moorselaar, J. Uff, A. Mahadevan-Jansen and N. Stone, *J. Photochem. Photobiol., B*, 2009, **95**, 170–176.
- 33 L. J. Livermore, M. Isabelle, I. M. Bell, O. Edgar, N. L. Voets, R. Stacey, O. Ansorge, C. Vallance and P. Plaha, *J. Neurosurg.*, 2021, **135**, 469–479.
- 34 I. P. Santos, P. J. Caspers, T. Bakker Schut, R. van Doorn, S. Koljenović and G. J. Puppels, *J. Raman Spectrosc.*, 2015, **46**, 652–660.
- 35 I. P. Santos, P. J. Caspers, T. C. Bakker Schut, R. van Doorn, V. Noordhoek Hegt, S. Koljenović and G. J. Puppels, *Anal. Chem.*, 2016, **88**, 7683–7688.
- 36 Y. Aaboubout, M. R. Nunes Soares, T. C. Bakker Schut, E. M. Barroso, M. van der Wolf, E. Sokolova, V. Artyushenko, A. Bocharnikov, I. Usenov, C. G. F. van Lanschot, L. Ottevanger, H. Mast, I. ten Hove, B. P. Jonker, S. Keereweer, D. A. Monserez, A. Sewnaik, J. A. U. Hardillo, R. J. Baatenburg de Jong, S. Koljenović and G. J. Puppels, Submitted, 2023.
- 37 B. Framery, M. Gutowski, K. Dumas, A. Evrard, N. Muller, V. Dubois, J. Quinonero, F. Scherninski, A. Pèleguin and F. Cailler, *Toxicol. Rep.*, 2019, **6**, 409–415.
- 38 M. Gutowski, B. Framery, M. C. Boonstra, V. Garambois, F. Quenet, K. Dumas, F. Scherninski, F. Cailler, A. L. Vahrmeijer and A. Pèleguin, *Surg. Oncol.*, 2017, **26**, 153–162.
- 39 I. Santos, *Improving Clinical Diagnosis of Melanocytic Skin Lesions by Raman Spectroscopy*, Ph.D. thesis, Erasmus University Rotterdam, 2018.
- 40 S. Keereweer, P. B. A. A. Van Driel, T. J. A. Snoeks, J. D. F. Kerrebijn, R. J. Baatenburg de Jong, A. L. Vahrmeijer, H. J. C. M. Sterenborg and C. W. G. M. Löwik, *Clin. Cancer Res.*, 2013, **19**, 3745–3754.
- 41 M. Leiloglou, V. Chalau, M. S. Kedrzycki, P. Thiruchelvam, A. Darzi, D. R. Leff and D. S. Elson, *J. Phys. D: Appl. Phys.*, 2021, **54**, 194005.
- 42 A. Johansson, G. Palte, O. Schnell, J.-C. Tonn, J. Herms and H. Stepp, *Photochem. Photobiol.*, 2010, **86**, 1373–1378.
- 43 M. Koch, P. Symvoulidis and V. Ntziachristos, *Nat. Photonics*, 2018, **12**, 505–515.
- 44 F. J. Voskuil, S. J. de Jongh, W. T. R. Hooghiemstra, M. D. Linssen, P. J. Steinkamp, S. A. H. J. de Visscher, K.-P. Schepman, S. G. Elias, G.-J. Meersma, P. K. C. Jonker, J. J. Doff, A. Jorritsma-Smit, W. B. Nagengast, B. van der Vegt, D. J. Robinson, G. M. van Dam and M. J. H. Witjes, *Theranostics*, 2020, **10**, 3994–4005.
- 45 P. J. Caspers, H. A. Bruining, G. J. Puppels, G. W. Lucassen and E. A. Carter, *J. Invest. Dermatol.*, 2001, **116**, 434–442.
- 46 I. P. Santos, E. M. Barroso, T. C. Bakker Schut, P. J. Caspers, C. G. F. van Lanschot, D.-H. Choi, M. F. van der Kamp, R. W. H. Smits, R. van Doorn, R. M. Verdijk, V. Noordhoek Hegt, J. H. von der Thüsen, C. H. M. van Deurzen, L. B. Koppert, G. J. L. H. van Leenders, P. C. Ewing-Graham, H. C. van Doorn, C. M. F. Dirven, M. B. Busstra, J. Hardillo, A. Sewnaik, I. ten Hove, H. Mast, D. A. Monserez, C. Meeuwis, T. Nijsten, E. B. Wolvius, R. J. Baatenburg de Jong, G. J. Puppels and S. Koljenović, *Analyst*, 2017, **142**, 3025–3047.
- 47 M. Paraskevaidi, B. J. Matthew, B. J. Holly, B. J. Hugh, C. P. V. Thulya, C. Loren, C. StJohn, G. Peter, G. Callum, K. G. Sergei, K. Kamila, K. Maria, L. M. G. Kássio, M.-H. L. Pierre, P. Evangelos, P. Savithri, A. A. John, S. Alexandra, S. Marfran, S.-S. Josep, T. Gunjan, W. Michael and W. Bayden, *Appl. Spectrosc. Rev.*, 2021, **56**, 804–868.